Mutation of Ser-50 and Cys-66 in Snapin Modulates Protein Structure and Stability

Aaron Navarro,[†] José A. Encinar,[†] Blanca López-Méndez,[‡] David Aguado-Llera,[†] Jesús Prieto,[§] Javier Gómez,[†] Luís Alfonso Martínez-Cruz,[‡] Oscar Millet,[‡] José Manuel González-Ros,[†] Gregorio Fernández-Ballester,[†] José L. Neira,[†,‖] and Antonio Ferrer-Montiel*,[†]

[†]Instituto de Biología Molecular y Celular, Universidad Miguel Hernández, 03202 Elche, Spain
[‡]Structural Biology Unit, CIC bioGUNE, 48160 Derio, Spain
[§]Departamento de Biología Estructural y Biocomputación, CNIO, 28029 Madrid, Spain
[‖]Complex Systems Physics Institute, 50009 Zaragoza, Spain

Ⓢ *Supporting Information*

ABSTRACT: Snapin is a 15 kDa protein present in neuronal and non-neuronal cells that has been implicated in the regulation of exocytosis and endocytosis. Protein kinase A (PKA) phosphorylates Snapin at Ser-50, modulating its function. Likewise, mutation of Cys-66, which mediates protein dimerization, impairs its cellular activity. Here, we have investigated the impact of mutating these two positions on protein oligomerization, structure, and thermal stability, along with the interaction with SNARE proteins. We found that recombinant purified Snapin in solution appears mainly as dimers in equilibrium with tetramers. The protein exhibits modest secondary structure elements and notable thermal stability. Mutation of Cys-66 to Ser abolished subunit dimerization, but not higher-order oligomers. This mutant augmented the presence of α-helical structure and slightly increased the protein thermal stability. Similarly, the S50A mutant, mimicking the unphosphorylated protein, also exhibited a higher helical secondary structure content than the wild type, along with greater thermal stability. In contrast, replacement of Ser-50 with Asp (S50D), emulating the protein-phosphorylated state, produced a loss of α-helical structure, concomitant with a decrease in protein thermal stability. In vitro, the wild type and mutants weakly interacted with SNAP-25 and the reconstituted SNARE complex, although S50D exhibited the strongest binding to the SNARE complex, consistent with the observed higher cellular activity of PKA-phosphorylated Snapin. Our observations suggest that the stronger binding of S50D to SNAREs might be due to a destabilization of tetrameric assemblies of Snapin that favor the interaction of protein dimers with the SNARE proteins. Therefore, phosphorylation of Ser-50 has an important impact on the protein structure and stability that appears to underlie its functional modulation.
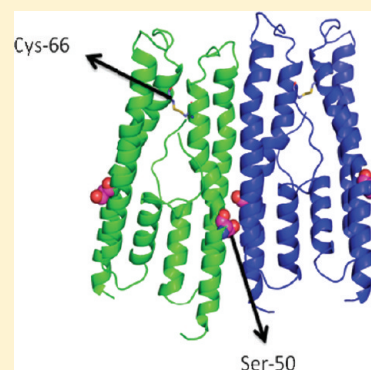
Regulated, Ca²⁺-triggered release of neurotransmitter from synaptic vesicles is mediated by the orchestrated assembly and disassembly of protein complexes between vesicular and plasma membrane proteins.[1,2] In general, these complexes are involved in the mobilization, docking, and fusion of cargo vesicles at the neuronal membrane. The SNARE complex is a biochemical intermediate formed before vesicle exocytosis that is crucial for vesicular docking and fusion processes.[3] In fact, it is currently accepted that assembly of the SNARE complex pulls the vesicle and plasma membrane together to initiate the fusion reaction upon receiving the activating Ca²⁺ signal.[1,4]

The SNARE complex is formed by the vesicular membrane protein synaptobrevin (also known as VAMP), and the plasma membrane proteins syntaxin and synaptosome-associated protein of 25 kDa (SNAP-25).[1,5] Several proteins have been shown to regulate the function of the SNARE complex by binding to one or several of the components in the assembly.[2] For complexin and Munc-18 proteins, the binding and the associated structural changes in the SNARE complex are well understood, and models have been proposed to describe how the assembly functions.[6,7] Similarly, a great advance has been made in the understanding of how the Ca²⁺ sensor synaptotagmin-I (Syt-I) operates.[8,9] These proteins are Ca²⁺-binding proteins of the synaptic vesicle membrane, which are necessary for maturation of synaptic vesicles.[10] Moreover, the interaction of Syt-I with SNAP-25 is critical for the release of dense-core vesicles and sensitization of the SNARE complex.[11,12] Therefore, the identification and structural characterization of molecular components involved in the assembly and disassembly of the SNARE complex are important for achieving a full understanding of the molecular mechanisms behind vesicle fusion.

Snapin is a 15 kDa protein that has been identified as a binding partner of SNAP-25 modulating the interaction of the

SNARE proteins with Syt-1.[13] The exact function of Snapin is yet being debated, because it seems to be involved in diverse processes, as suggested by its ubiquitous expression and subcellular location in both the cytosol and the plasma membrane.[13−15]

Phosphorylation of Snapin at Ser-50 by PKA in cells strengthens its association with the SNARE complex.[16] Moreover, inhibition of Snapin phosphorylation in vivo by estrogen receptor-binding fragment-associated gene 9 reduces the level of exocytosis of synaptic vesicles.[15] In hippocampal neuron autapses, synaptic transmission is also regulated by Snapin.[17] Recently, it was reported that this protein facilitates synchronization of synaptic vesicle function.[18] Participation in the endocytotic pathway has also been suggested.[19] Note-worthy, in addition to SNARE proteins, is the fact that Snapin binds to a plethora of cellular proteins, including SNAP-23 and transient receptor potential (TRP) channels.[20−22] Therefore, these observations imply that Snapin, like other SNARE regulatory proteins,[23] plays a modulatory role in vesicle trafficking, dockingm and/or fusion in both regulated and constitutive exocytosis.

Despite the functional relevance of Snapin, data about its structure and conformational stability are limited, and its binding to SNAP-25 appears to be controversial. Theoretical structural prediction algorithms suggest that Snapin is composed of two domains: a hydrophobic N-terminal segment and a C-terminal coiled-coil region.[13] Structurally, Snapin appears to be an α-helical dimeric protein that unfolds cooperatively and reversibly.[14] This study, however, could not detect in vitro binding of Snapin to SNAP-25, at variance with results reported by other groups.[13,18,23] Recently, a Snapin mutant (C66A) that abrogates disulfide-mediated dimerization of the protein was reported to have a significantly lower affinity for binding to SNAP-25 and Syt-I,[18] suggesting that the oligomeric state of Snapin may be important for interacting with partner proteins.

Here, we investigate the structural and conformational features of wild-type Snapin along with a C66S mutant that eliminates disulfide-mediated dimerization and S50A and S50D mutants that mimic the constitutive unphosphorylated and phosphorylated states of the protein, respectively. To character-ize the structure and stability of Snapin and its mutants, we used circular dichroism (CD), nuclear magnetic resonance (NMR), and Fourier transform infrared spectroscopy (FTIR). Our results show that both wild-type Snapin and the C66S mutant are oligomeric proteins in solution. The wild-type protein assembles primarily as dimers and tetramers, while the C66S mutant forms mainly tetramers. Mutation of Cys-66 to Ser significantly increases the content of helical secondary structure, leading to an increase in the thermal stability of the protein. Mutation of Ser-50 to Ala also resulted in a notable increase in the content of protein secondary structure and thermal stability. In contrast, replacement of Ser-50 with Asp notably reduced the content of helical structure and decreased the thermal stability of the protein. The wild type and mutants modestly interacted in vitro with purified SNAP-25 (<20%) and exhibited slightly stronger binding to the reconstituted SNARE complex composed of SNAP-25, VAMP2, and Syntaxin (~24%). Mutant S50D displayed the higher level of interaction with the SNARE proteins. These results imply that abrogation of Snapin dimerization modestly impacts the structure and stability of the protein by favoring the assembly of tetramers. In contrast, phosphorylation of Ser-50 might destabilize the formation of protein tetramers, a process that could be important in favoring the interaction of dimers with the SNARE complex, thus stimulating vesicle exocytosis.

■ EXPERIMENTAL PROCEDURES

Materials. Standard suppliers were used for all chemicals. Water was deionized and purified on a Millipore system.

Cloning and Mutagenesis of Snapin. The cDNA encoding full-length Snapin was cloned into the pET22b vector (Invitrogen), to express the protein with a six-His tag at the C-terminus. Site-directed mutagenesis of the Cys-66 to Ser, Ser-50 to Ala, and Ser-50 to Asp single mutants was conducted using the QuikChange site-directed mutagenesis kit (Strata-gene), as described previously.[24]

Expression and Purification of Snapin and SNARE Proteins. His-tagged Snapin and mutants (C66S, S50A, and S50D) were produced in *Escherichia coli* strain C41 that successfully express membrane proteins or, alternatively, proteins with a large amount of hydrophobic patches.[25] Protein expression was induced with 1 mM IPTG when the culture reached an OD_{600} of 0.6−0.8 for 16−24 h at 37 °C. Cells were centrifuged at 6000 rpm in a Beckman Coulter J2-HS centrifuge for 15 min and frozen at −80 °C until they were used. The cell pellet from 8 L of culture was resuspended in lysis buffer [500 mM NaCl, 5 mM imidazole, 20 mM Tris (pH 8.0), 0.1% Triton X-100, and 1 mM β-mercaptoethanol (β-MSH)], supple-mented with one tablet of Complete-EDTA-free protease inhibitors (Roche), and sonicated 10 times in ice with bursts of 45 s at maximal power (model 102-C, Branson), interleaved with 15 s in ice. The homogenate was centrifuged at 15000 rpm for 50 min in a Beckman Coulter J2-HS centrifuge. The supernatant was poured onto 5 mL of Ni-NTA (GE Healthcare) for affinity purification.

The extract/resin mixture was kept in a cold room under agitation for 30 min. The suspension was added to a column sleeve (Bio-Rad), and the resin was separated from the buffer by gravity. A volume of 20 mL of washing buffer [500 mM NaCl, 30 mM imidazole, 20 mM Tris (pH 8.0), and 1 mM β-MSH] was added and the mixture left for 20 min at room temperature; every 5 min, resin and buffer were allowed to mix by agitation. The washing buffer was separated from the resin by gravity. Elution buffer [500 mM NaCl, 300 mM imidazole, 20 mM Tris (pH 8.0), and 1 mM β-MSH] was added to the resin, and the flow-through was collected immediately. The eluted protein was concentrated using Amicon centrifugal devices (Millipore) with a molecular mass cutoff of 3 kDa and loaded onto a G-75 Superdex 16/60 column (GE Healthcare) running on an AKTA-FPLC system (GE Healthcare) by following the absorbance at 280 nm. The column was equilibrated in 50 mM Tris (pH 7.4) with 150 mM NaCl. The protein purity was higher than 95%, as judged from sodium dodecyl sulfate−polyacrylamide gel electrophoresis (SDS−PAGE) gels. Because of the high content of positively charged amino acids, we tested whether the protein contained any bound DNA by running a 5% agarose gel (data not shown). Approximately 10−15 mg of protein per liter of culture was obtained. The protein concentration was determined from the absorbance using the extinction coefficient of tyrosine residues.[26] Absorbance measurements were taken in a Shidmazu UV-1601 ultraviolet spectrophotometer, using a 1 cm path-length cell (Hellma). The protein was kept at −80 °C in 50 mM Tris and 150 mM NaCl (pH 7.4) until it was used. Attempts to express in ^{15}N minimal medium either Snapin or

the C66S mutant, by using the same protocol described for other proteins,[27] failed because both Snapin species accumulated as inclusion bodies.

The recombinant expression and purification of GST-SNAP-25 (full-length rat SNAP-25), GST-VAMP2 (cytosolic domain rat VAMP2), and GST-syntaxin (cytosolic domain rat syntaxin 1a) were performed as previously described.[28] To obtain the proteins, the GST fusion protein was treated with thrombin for 2 h at 25 °C. Approximately 1−10 mg of proteins per liter of culture was obtained and stored at −80 °C until it was used.

For pull-down experiments, equimolar amounts (2.5 μM) of Snapin-His bound to NTA-Ni or His mutants and SNAP-25 or preassembled SNARE complex in 50 mM Tris (pH 7.5), 30 mM imidazole, and 0.1% Triton X-100 were incubated at 37 °C for 2 h; the resin was washed, and bound SNAP-25 was eluted with SDS−PAGE denaturing buffer and analyzed in 14% gels. Gels were digitized with a Chemlite 200 FA luminant image analysis system (Avagene Lite Science), and the area of the protein bands was analyzed using the GelVista and 1D gel image analysis software packages.

Fluorescence Measurements. Fluorescence spectra for both Snapin proteins were recorded on a Cary Eclipse spectrofluorometer (Varian) interfaced with a Peltier temperature control system. The sample concentration was in the range of 1−2 μM in PBS [10 mM phosphate (pH 7.0) and 150 mM NaCl]. A 1 cm-path-length quartz cell (Hellma) was used. Unless otherwise indicated, the experiments were performed at 25 °C.

For binding experiments, increasing amounts of SNAP-25, in the range of 0−30 μM, were added to a solution with a fixed concentration (4.7 μM in monomer units) of Snapin or the C66S mutant in PBS buffer. Samples were left overnight at 4 °C. The fluorescence of the resulting samples was measured after incubation for 2 h at 37 °C. Experiments were conducted with excitation at 280 and 295 nm, and emission fluorescence was collected between 300 and 400 nm. The excitation and emission slits were 5 nm, and the data pitch interval was 1 nm. The dissociation constant of the complex was calculated by fitting the observed changes in fluorescence intensity at a particular wavelength or in $\langle \lambda \rangle$ (average energy) versus the concentration of added SNAP-25 to the following equation

$$F_{meas} = F + \Delta F_{max} \times 0.5\left(C - \sqrt{C^2 - 4[A][B]}\right)$$

where F_{meas} is the measured fluorescence after subtraction of the blank, ΔF_{max} is the change in the fluorescence measured at saturating SNAP-25 concentrations, F is the fluorescence in the absence of SNAP-25, [A] denotes the SNAP-25 concentration, B denotes the Snapin concentration, and C represents [A] + [B] + K_D, where K_D is the dissociation constant. Job's method was used to determine the stoichiometry of the reaction.[29] Inner-filter effects at 280 and 295 nm were corrected for the absorbance of SNAP-25.

Circular Dichroism. Circular dichroism spectra of Snapin proteins were collected on a Jasco J810 spectropolarimeter fit with a thermostated cell holder and interfaced with a Neslab RTE-111 water bath. The instrument was periodically calibrated with (+)-10-camphorsulfonic acid. Isothermal wavelength spectra at different pHs were acquired at a scan speed of 50 nm/min with a response time of 2 s and averaged over six scans at 25 °C. Near-UV spectra were acquired by using 30−40 μM protein in 50 mM Tris (pH 7.4) in a 0.5 cm path-length cell. Far-UV measurements were performed with 5−100 μM

Snapin or mutants in 50 mM Tris (pH 7.4) using 0.1 or 0.2 cm path-length quartz cells (Hellma). All spectra were corrected by subtracting the proper baseline. The molar ellipticity, $[\Theta]$, and the α-helical content of the protein were calculated as described previously.[30,31] For dithiothreitol (DTT) treatment, Snapin wild-type protein was equilibrated in 50 mM Tris (pH 7.4) supplemented with 1 mM DTT at 4 °C overnight. Spectra of Snapin with SNAP-25 were recorded with the same set of parameters described above, and protein concentrations were 15 μM.

Fourier Transform Infrared Spectroscopy. The proteins were back-exchanged in deuterated buffer at the desired pH; no pH corrections were used for the isotope effects. Samples of Snapin or the C66S mutant, at a final concentration of 1 mM, were placed between a pair of CaF$_2$ windows separated by a 50 μm thick spacer, in a Harrick demountable cell. Spectra were acquired on a Bruker IF66s FTIR instrument equipped with a DTGS detector and thermostated with a Braun water bath at the desired temperature. The cell container was filled with dry air. Five hundred scans per sample were taken, averaged, apodized with a Happ−Genzel function, and Fourier transformed to give a final resolution of 2 cm^{-1}. The signal:noise ratio of the spectra was better than 10000:1. Buffer contributions were subtracted, and the resulting spectra were used for analysis. Band decomposition of the original amide I' has been described previously.[32] Briefly, protein secondary structure components were quantified from curve fitting analysis by band decomposition of the original amide I band after spectral smoothing. Spectral smoothing was conducted by applying the maximal entropy method, assuming that noise and band shape follow a normal distribution. The resulting spectra possess a signal:noise ratio of >10000:1. Derivation of IR spectra was performed using a power of 3 and a breakpoint of 0.3, and Fourier self-deconvolution was performed using a Lorenztian bandwidth of 18 cm^{-1} and a resolution enhancement factor (k) of 2.0. To quantify the secondary structure, we took the number and position of the absorbance band components from the deconvoluted spectra and estimated the bandwidth from the derived spectra and the absorbance height from the original spectra. The iterative curve fitting process was performed in CURVEFIT running under SpectraCalc (Galactic Industries Corp., Salem, NH). The number, position, and band shape were kept fixed during the first 200 iterations. The fittings were further refined by allowing the band positions to vary for 50 additional iterations. The goodness of fit between experimental and theoretical spectra was assessed from the χ^2 values (2×10^{-5} to 6×10^{-6}). The area of the fitted absorbance band components was used to calculate the percent of secondary structure. The error of the estimated percentage of secondary structure depends mainly on the removal of spectral noise, which was estimated to be 5%.[33]

Thermal Denaturation Measurements. Thermal denaturations of Snapin and mutants were performed at a constant heating rate of 60 °C/h and with a response time of 8 s. Thermal scans were collected in the far-UV region by following the ellipticity at 222 nm from 5 to 95 °C in 0.1 cm path-length quartz cells (Hellma) with a total protein concentration of 15 μM. The possibility of drifting of the CD spectropolarimeter was tested by running two samples containing only buffer, before and after the thermal experiments. No difference was observed between the scans. Every thermal denaturation experiment was repeated at least three times with new samples.

Analysis of thermal denaturations was conducted using a two-state mechanism.

Protein thermal melting was also monitored by FTIR by following the changes induced in the amide I′ band by temperature. Protein denaturation was characterized in D_2O by the appearance of two bands around 1616 and 1685 cm^{-1}, which are the result of intermolecular protein–protein contacts. The extent of protein thermal denaturation was determined by the ratio of the absorbances measured at 1616 and 1645 cm^{-1}. The thermal midpoint, T_m, was determined by using a two-state folding mechanism[32] following the changes in the absorbance ratio at two wavenumbers.

NMR Spectroscopy. The NMR experiments were conducted on Bruker Avance DRX-500 and III DRX-800 spectrometers (Bruker GmbH) equipped with triple-resonance and cryogenic-resonance probes, respectively, and z-pulse field gradients. Unless otherwise stated, all the experiments were conducted at 25 °C.

NMR samples were prepared by dissolving either Snapin or the C66S mutant in a 9:1 H_2O/D_2O solution, in phosphate buffer (50 mM, pH 7.0) at a final concentration of 80 μM. The sample was centrifuged briefly to remove insoluble protein and then transferred to a 5 mm NMR tube. Homonuclear one-dimensional (1D) NMR spectra were acquired using 16K data points averaged over 512 scans and a 10401.3 Hz spectral width (13 ppm), with the residual water signal removed by the WATERGATE sequence.[34] Data were zero-filled, resolution-enhanced, and baseline corrected with XWINNMR (Bruker GmbH) working on a personal computer. Spectra were referenced to external TSP.

Translational self-diffusion measurements were performed in a DRX-500 magnet with the pulsed gradient spin–echo as described previously.[35] The duration of the gradient was varied between 2.2 and 3 ms, and the time between both gradients was changed from 100 to 150 ms. The most upfield-shifted methyl groups were used to measure the changes in intensity in the spectra of Snapin and the C66S mutant. The gradient strength was calibrated by using the translational diffusion coefficient (D) for the residual proton water line in a sample containing 100% D_2O in a 5 mm tube, as described previously.[35] The D of the proteins was determined by using the approach described by Dobson and co-workers.[36] Briefly, the D of the protein is determined by comparison, under the same solution conditions, of the measured D for a standard compound (dioxan).

Analytical Ultracentrifugation (AU). The sedimentation velocity experiment was conducted in an XL-A analytical ultracentrifuge (Beckman-Coulter Inc.) at 42000 rpm and 20 °C, using an An50Ti rotor and a 12 mm charcoal-filled Epon double-sector centerpiece. Absorbance was measured at 280 nm. The protein concentration was 150 μM in 50 mM Tris (pH 8.0). Data were modeled as a superposition of Lamm equation solutions with SEDFIT (available at http://www.anlyticalultracentrifugation.com/default.htm).[37] The sedimentation coefficient distribution, $c(s)$, was calculated at a $p = 0.68$ confidence level. The experimental sedimentation values were determined by integration of the main peak of $c(s)$ and corrected to standard conditions to obtain the corresponding $s_{20,w}$ values with SEDNTERP.[38] Calculation of the frictional coefficient ratio was performed with SEDFIT to obtain the $c(M)$ distribution.[37]

Sedimentation equilibrium experiments were performed at 20 °C in an Optima XL-A (Beckman-Coulter Inc.) analytical ultracentrifuge equipped with UV–visible optics, using an An50Ti rotor, with a 12 mm double-sector charcoal-filled Epon centerpiece. Samples of freshly dialyzed protein at 150 μM in 50 mM Tris-HCl (pH 8.0) were loaded into the cell, and the dialysate was transferred to the reference sector. High concentrations were necessary because of the small absorption coefficient of Snapin, because it has only two tyrosine residues. The short column (90 μL) for sedimentation equilibrium was used at 21000 rpm, and the system was assumed to be at equilibrium when the successive scans overlaid. The equilibrium scans were obtained at 280 nm. The baseline signal was measured after high-speed centrifugation (5 h at 42000 rpm). The whole-cell apparent molecular weight of the protein was obtained with EQASSOC,[39] and the goodness of fit was judged by the values of residuals (in all cases within less than ±0.02).

■ RESULTS

Recombinant Snapin and the C66S Mutant Are Oligomeric Proteins in Solution. Gel filtration chromatography shows that both proteins eluted as two discernible peaks at 44 and 59 mL in a Superdex G75 16/60 column that corresponded to a molecular mass of ≈60 kDa (Figure 1A). We did not observe differences in the Snapin chromatogram when the wild-type protein was incubated with 1 mM dithiothreitol (DTT) (data not shown), in agreement with the chromatographic profile of the C66S mutant. Accordingly, we conducted the experiments in the absence of any reducing agent. These elution volumes were close to that of albumin (67 kDa), implying that both protein species assemble as similar oligomers, presumably tetramers. Note that the oligomeric assemblies are SDS-sensitive, giving rise to monomers and dimers in the presence of the chaotropic agent (Figure 1B). Furthermore, our findings indicate that Snapin oligomerization is independent of the formation of stable, disulfide-mediated dimers, because the C66S mutant multimerizes in the absence of covalent-mediated protein dimerization (Figure 1B). Additional insights into Snapin multimerization were gained from the concentration dependence of the molar ellipticity per residue that changed from −4034 deg cm^2 $dmol^{-1}$ at 5 μM to −4478 deg cm^2 $dmol^{-1}$ at 100 μM, suggesting the occurrence of protein self-association in solution[31,40] (data not shown). Accordingly, these findings suggest that recombinant Snapin in solution forms homooligomers.

To further characterize the oligomeric state of the protein, we next evaluated the shape of Snapin in solution by using DOSY-NMR. The translational diffusion coefficient (D) from the DOSY-NMR measurements for Snapin was $(4.9 \pm 0.2) \times 10^{-7}$ cm^2 s^{-1} (either in the absence or in the presence of DTT), and that of dioxan under the same conditions was $(8.31 \pm 0.04) \times 10^{-6}$ cm^2 s^{-1}, which, because the R_S of dioxan is 2.12 Å,[36,41] yielded an R_S of 35.7 Å for Snapin; for the C66S mutant, the measured values were similar, with a D of $(5.3 \pm 0.2) \times 10^{-7}$ cm^2 s^{-1} and an R_S of 36.5 Å. The hydrodynamic radius, R_t, for a nonsolvated spherical molecule can be calculated as $R_t = [(3M\bar{V})/(4N\pi)]^{1/3}$,[42] where $\bar{V}$ is the specific volume (0.74 cm^3/g for Snapin), N is Avogadro's number, and M is the molecular mass (15939 Da for Snapin). For monomeric wild-type Snapin, an R_t of 16.7 Å was obtained, which is significantly smaller than that measured experimentally (35.7 Å), thus suggesting that Snapin is an oligomer in solution (a similar value was obtained for the C66S mutant). Alternatively, both proteins may display a rather elongated shape in solution, yielding a large hydrodynamic radius. Indeed, it must be kept in mind that the measured D value for both Snapin species
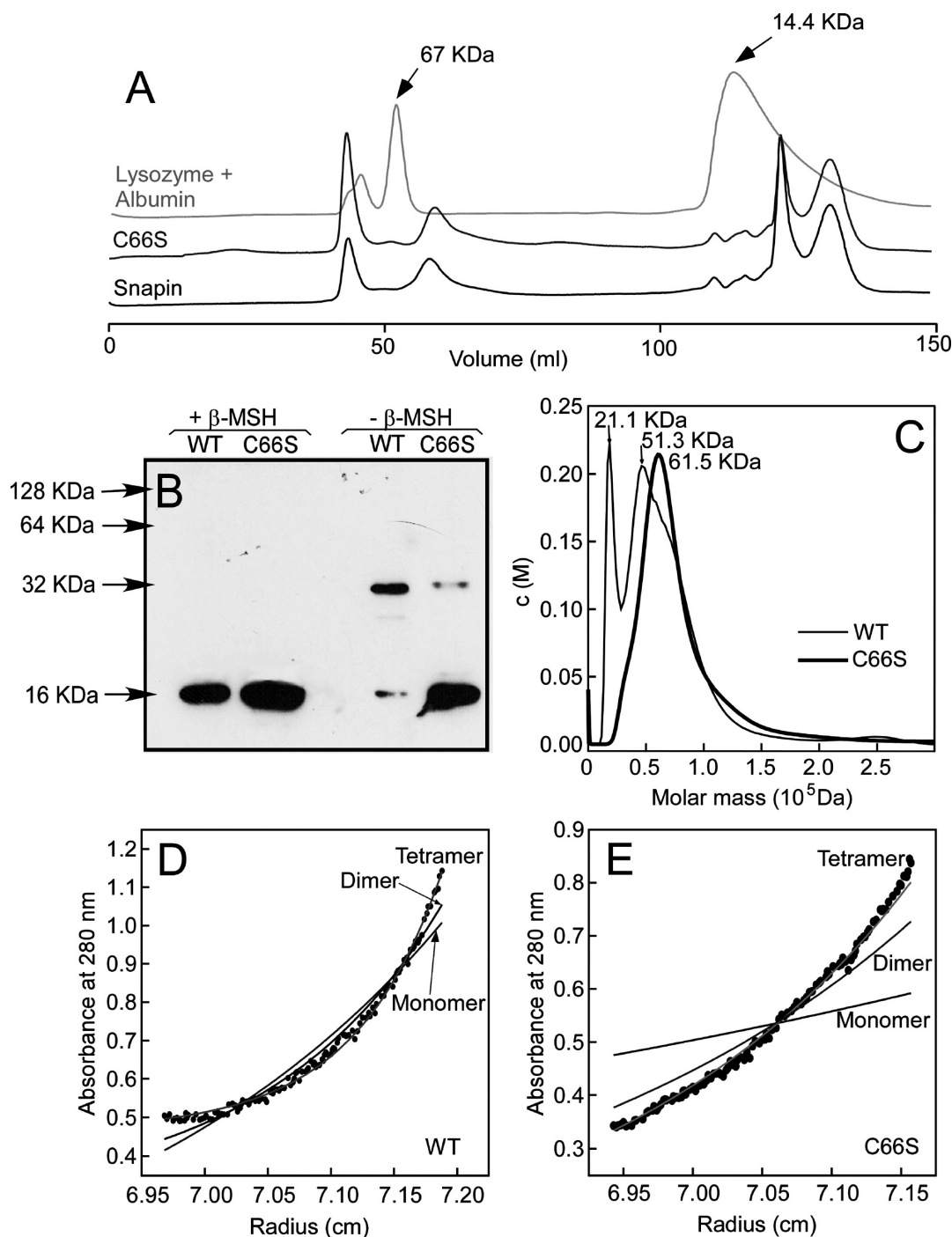
Figure 1. Recombinant Snapin and the C66S mutant form multimers in solution. (A) Size-exclusion chromatograms of both protein species in comparison to those of lysozyme and albumin. Purified proteins were eluted from a Superdex-75 16/60 column coupled to an absorbance UV detector. Proteins were loaded in phosphate buffer (pH 7.0) and 150 mM NaCl at a concentration of 5 mg/mL. Lysozyme and albumin were loaded at 3 mg/mL each. (B) SDS−PAGE analysis of Snapin and the C66S mutant under reducing (+β-MSH) and nonreducing (−β-MSH) conditions. Proteins (5 μg) were separated in a 12% gel. (C) Sedimentation velocity analysis of Snapin and the C66S mutant at 42000 rpm and 20 °C. (D and E) Sedimentation equilibrium experiments with Snapin and the C66 mutant, respectively. Solid lines depict the best fits to a monomeric, dimeric, and tetrameric species. The sedimentation equilibrium displayed was obtained at 21000 rpm and 25 °C. The protein concentration was 150 μM. All experiments were conducted in the absence of reducing agents unless specified as in panel B.

is the weighted average of all species in solution, and then, it contains contributions of all possible multimeric assemblies with any shape in fast equilibrium on the NMR time scale. Further support to the self-association of both Snapin proteins comes from studies of Dobson and co-workers;[36] they have suggested that the R_S of a folded globular protein is given by $(4.75 \pm 1.11)N_u^{0.29}$, where N_u is the number of residues. This approach yields an R_S of 20 ± 4 Å for monomeric Snapin. Noteworthy is the fact that a tetrameric Snapin protein would yield an R_S of 30 ± 5 Å, which is similar to that inferred from the weight-average diffusion coefficient.

To obtain a better estimate of the oligomeric state, we used analytical ultracentrifugation (AU) to determine the molar mass of all species in solution and the association state of the macromolecules.[37] Sedimentation velocity results showed that Snapin solutions had a peak of 21.1 kDa and a broad peak centered at 51.3 kDa, with a pronounced shoulder at 60 kDa (Figure 1C). In contrast, the C66S mutant solution displayed a distribution of mass along the cell that could be fit to a solute with an apparent molecular mass of 61.5 kDa (Figure 1C), very close to the calculated value of 63.7 kDa for a tetrameric protein. Similarly, sedimentation equilibrium experiments revealed mainly the presence of dimers and tetramers in the Snapin solution (Figure 1D) and tetramers for the C66S mutant (Figure 1E). Because sedimentation equilibrium and velocity measurements are more appropriate approaches for molecular mass determination than size-exclusion chromatography or DOSY-NMR measurements, we conclude that wild-type Snapin is a mixture of dimers and tetramers, while the C66S mutant forms mainly stable tetramers. Taken together, our findings suggest that Snapin tetramerization is probably mediated by the formation of coiled coils and does not depend on the formation of an intersubunit disulfide bond between Cys-66 residues, because these multimers were also observed in the dimerization-defective protein.

Mutation of Cys-66 to Ser Increases the Helical Secondary Structure Content of the Protein. We next investigated the secondary and tertiary structural features of Snapin and the C66S mutant. For this task, we employed complementary spectroscopic approaches, including fluorescence, CD, NMR, and FTIR. The near-UV spectrum of both proteins was very weak and did not show any particular feature probably because of the low content of aromatic residues (two tyrosines and two phenylalanines). Similarly, the fluorescence spectrum yielded a maximum at 307 nm, which is characteristic of a protein with only tyrosine residues.

The far-UV CD spectra of Snapin and the C66S mutant at 15 μM displayed minima at 208 and 222 nm and a maximum at 195 nm (Figure 2A). The molar ellipticity of the wild-type protein was low and consistent with a modest content of α-helical secondary structure. In contrast, the spectrum of the C66S mutant was approximately 2-fold more intense than that of Snapin, suggesting a higher α-helical content. Note that the intensity of the 222 nm peak is slightly higher than that at 208 nm [$\theta_{222}/\theta_{208} \approx 1.09$ (Figure 2A)], consistent with the presence of oligomeric species in the solution.[43] The deconvolution of the far-UV spectra by the DICHROWEB algorithm[44,45] yielded an average α-helix content of 16−20% for Snapin that was increased to 30−35% for the C66S mutant (Figure 2B). Intriguingly, the far-UV CD spectrum of wild-type Snapin in the presence of 1 mM DTT did not show any difference in the percentage of secondary structures (data not shown). Similarly, an increase in the concentration of NaCl from 30 to 300 mM did not result in a significant increase in the α-helical content of the wild-type protein.

To further characterize the elements of secondary structure, we studied both proteins by FTIR. At variance with CD, FTIR requires a protein concentration of 1 mM. As depicted in panels C and D of Figure 2, the C66S mutant showed a maximum centered at 1650 cm^{-1}, characteristic of a significant α-helical secondary structure content. Self-deconvolution of the infrared spectrum revealed a 70% α-helix content (Figure 2D). In contrast, the wild-type protein displayed the maximum centered at 1680 cm^{-1}, consistent with a lower (35−40%) α-helical

content (Figure 2C). Akin to CD measurements, incubation of wild-type protein with 2.5 mM DTT did not alter the percentage of α-helix in the wild-type protein (data not shown). The higher structural order of the C66S mutant was further substantiated by hydrogen exchange experiments of the amide II band that revealed the lack of this band in wild-type Snapin. In contrast, we observed the presence of a residual amide II band in the C66S mutant after the protein had been dissolved in D$_2$O for 85 min (Figure S1, Supporting Information), consistent with a more rigid secondary structure in the mutant than in the wild-type protein. Note that the higher α-helical content inferred from the infrared spectra likely arises from the higher concentration of protein used with this technique that may promote protein oligomerization. An increase in the protein concentration will favor the formation of self-associated species. Nonetheless, independent of the quantitative estimates, both techniques indicate that mutation of Cys-66 to Ser induces a significant increase in the secondary structure content of the protein. Because C66S is present as tetrameric assemblies, these findings imply that tetramers are more structured species than dimers.

The homonuclear 1D NMR spectra of Snapin and the C66S mutant further corroborated the finding that these proteins display secondary structure in solution as evidenced by the dispersion in the amide region (Figure 2E), and the upfield-shifted methyl groups (Figure 2F). The spectra resemble those of a modestly structured chain with the amide resonances dispersed between 7.5 and 8.5 ppm, and all the methyl protons of valines, isoleucines, and leucines close to 0.8 ppm.[46] Two-dimensional ^{15}N HSQC NMR spectra could not be acquired because both ^{15}N-labeled proteins accumulated in inclusion bodies when they were grown in minimal media (see Experimental Procedures). All these observations are in agreement with the CD and FTIR measurements and demonstrate that these proteins display α-helix secondary structure, which is enhanced by mutation of Cys-66 to Ser.

Thermal Stabilities of Snapin and the C66S Mutant. To gain insights into the stability of both protein species, we studied their thermal unfolding at low (micromolar) and high (millimolar) concentrations by CD and FTIR, respectively (Figure 3). Thermal melting curves, followed as the change in ellipticity at 222 nm in the far-UV CD for both wild-type Snapin and the C66S mutant at 15 μM, exhibited sigmoidal behavior with midpoint temperatures (T_m) of 57.9 $\pm$ 0.3 °C for Snapin and 60.1 $\pm$ 0.2 °C for the C66S mutant (Figure 3A). The presence of 1 mM DTT did not shift the T_m of the wild type (data not shown). The 2 °C higher T_m of the C66S mutant is consistent with a higher helical content and, thus, a more rigid secondary structure.

At a high concentration (1 mM), thermal denaturations were followed by the changes in the 1616 cm^{-1} to 1645 cm^{-1} absorbance ratio of amide I' in the FTIR spectra for both proteins (Figure S2, Supporting Information). Melting curves revealed that wild-type Snapin exhibited a T_m of 71 °C and while the C66S mutant showed a T_m of 72.4 °C (Figure 3B), in agreement with the higher content of structure displayed by both proteins at the millimolar concentration. This is further substantiated by the stronger cooperativity of the melting process observed at high protein concentrations.

To further evaluate the thermal stability of the proteins, we investigated whether the heat-induced unfolding at micromolar concentrations was reversible by looking at the protein refolding. For this purpose, we applied two consecutive heat
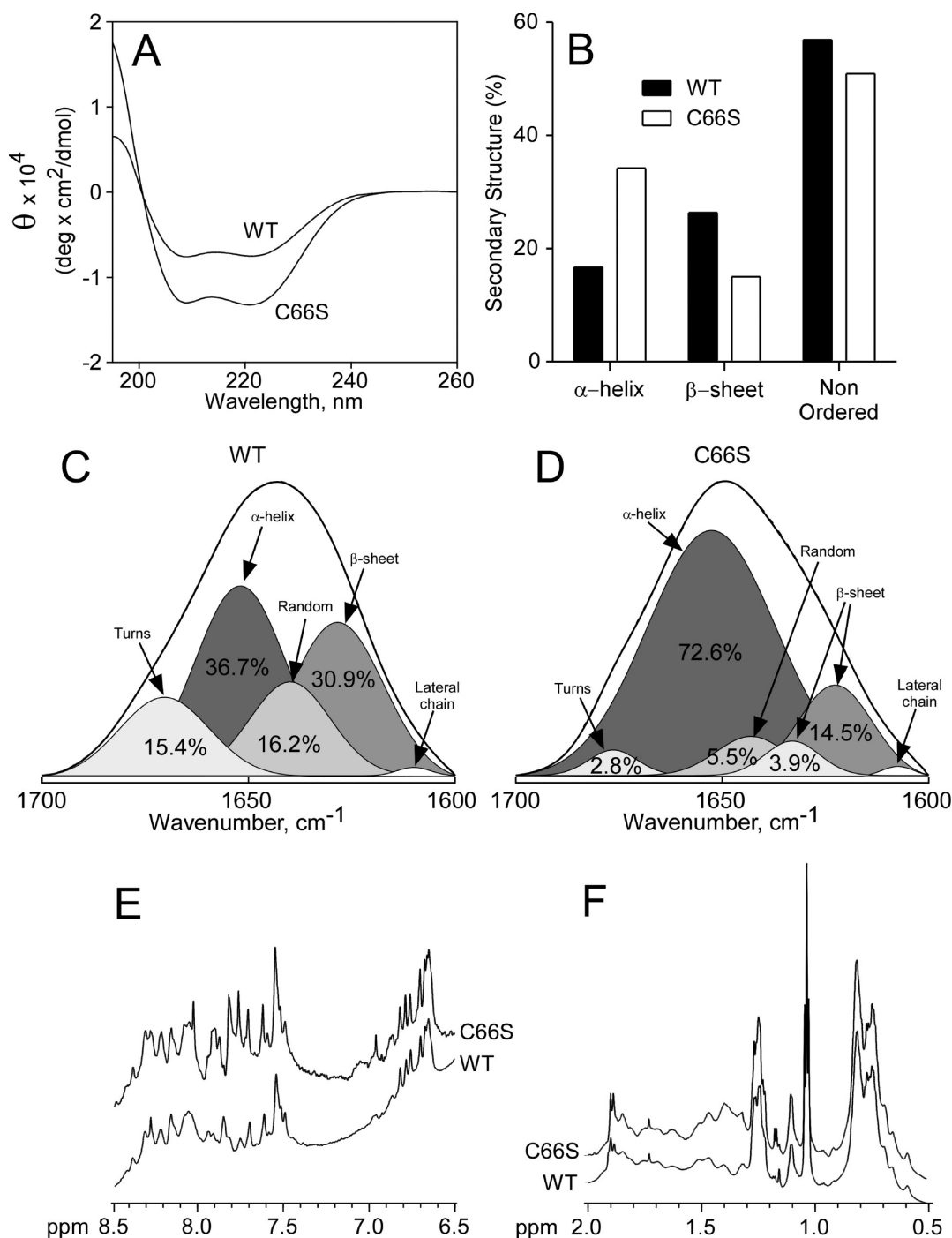
Figure 2. Structural characterization of Snapin and the C66S mutant. (A) Far-UV CD spectra of the wild type and the C66S mutant in phosphate buffer (pH 7.0). The protein concentration was 15 μM. (B) Percentage of secondary structure elements inferred from the CD spectra determined using the DICHROWEB algorithm. (C and D) FTIR spectra of Snapin and the C66S mutant in phosphate buffer (pH 7.0). The protein concentration was 1.0 mM. The spectra were deconvoluted in the percentages of secondary structure elements, displayed as individual Gaussian-like graphs. (E) Homonuclear 1D NMR spectra of the amide and aromatic regions for wild-type Snapin and its C66S mutant. (F) Methyl regions of the 1D NMR spectrum of Snapin and the C66S mutant. Conditions were 20 °C and phosphate buffer (pH 7.3). The protein concentration for NMR was 80 μM.

ramps interspersed with a cooling period. As illustrated in panels C and D of Figure 3, the CD spectrum of a reheated sample of the wild-type protein and the C66S mutants was virtually identical to that obtained before the proteins were heated to 95 °C, revealing a minimal loss of protein (5−8%). Furthermore, neither the sigmoidal shape of the unfolding curve nor the T_m (56.9 °C for the wild type and 59.9 °C for

C66S) was significantly altered in the second heat ramp (Figure 3E,F), indicating that the thermal denaturation of both proteins is a reversible process and that both species are thermally stable.

Mutation of Ser-50 Modulates the Structure and Thermal Stability of Snapin. It has been reported that Snapin is a substrate of PKA that phosphorylates the protein at residue Ser-50.[16] PKA-induced phosphorylation of Snapin
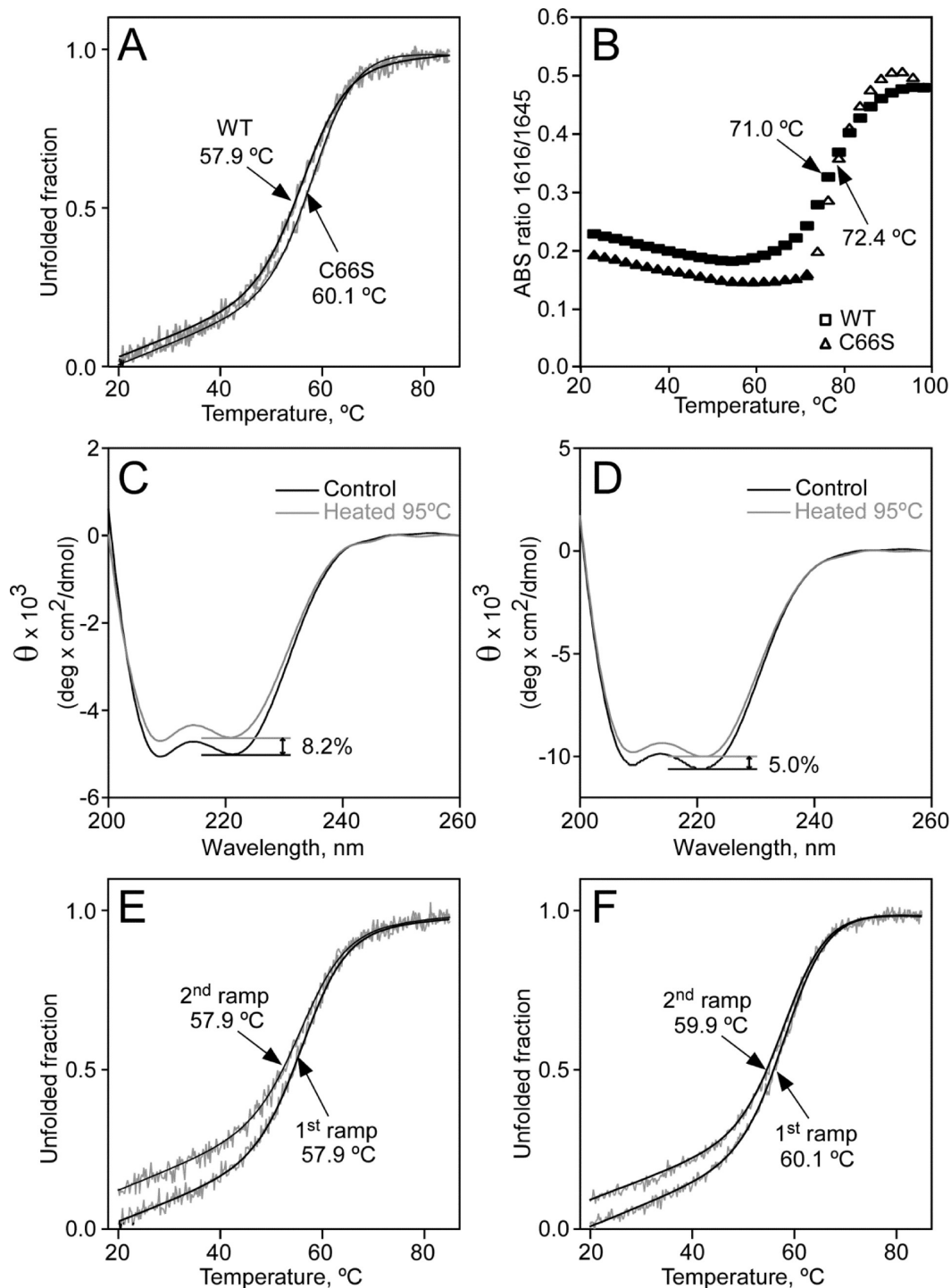
Figure 3. Thermal denaturation of Snapin proteins monitored by CD and FTIR. (A) Normalized fraction of the unfolded protein during the thermal denaturation of Snapin and the C66S mutant obtained by following the changes in ellipticity at 222 nm (far-UV CD). Thermal denaturation was measured at a thermal rate of 60 °C/h. The protein concentration was 15 μM in 50 mM Tris (pH 7.4). (B) Thermal unfolding measured by FTIR as the change in the ratio of band intensities at 1616 and 1645 cm^{-1} at increasing temperatures. The protein concentration was 1.0 mM. The T_m of each sigmoidal transition was calculated by fitting the curves to a two-state model. (C and D) Thermal denaturation of native (black) and refolded proteins (gray), monitored by following the ellipticity at 222 nm of wild-type Snapin and the C66S mutant, respectively. Refolded proteins refer to a protein sample that has been thermally denatured using a ramp protocol and refolded by being incubated at 25 °C. (E and F) Normalized unfolded protein as a function of thermal melting and refolding for the wild type and C66S mutant, respectively.

results in stronger binding to synaptotagmin and the SNARE complex, stimulating neurosecretion.[16] Modulation of Snapin functionality by chemical modification of Ser-50 implies the potential induction of structural changes in the protein. Thus, we next evaluated the structural and stability impact of

mutating Ser-50 to Ala, mimicking the constitutive unphosphorylated form of the protein, and to Asp, to emulate the constitutively phosphorylated species. Both mutants were recombinantly produced, displaying a chromatographic profile identical to that of the wild-type protein (data not shown).
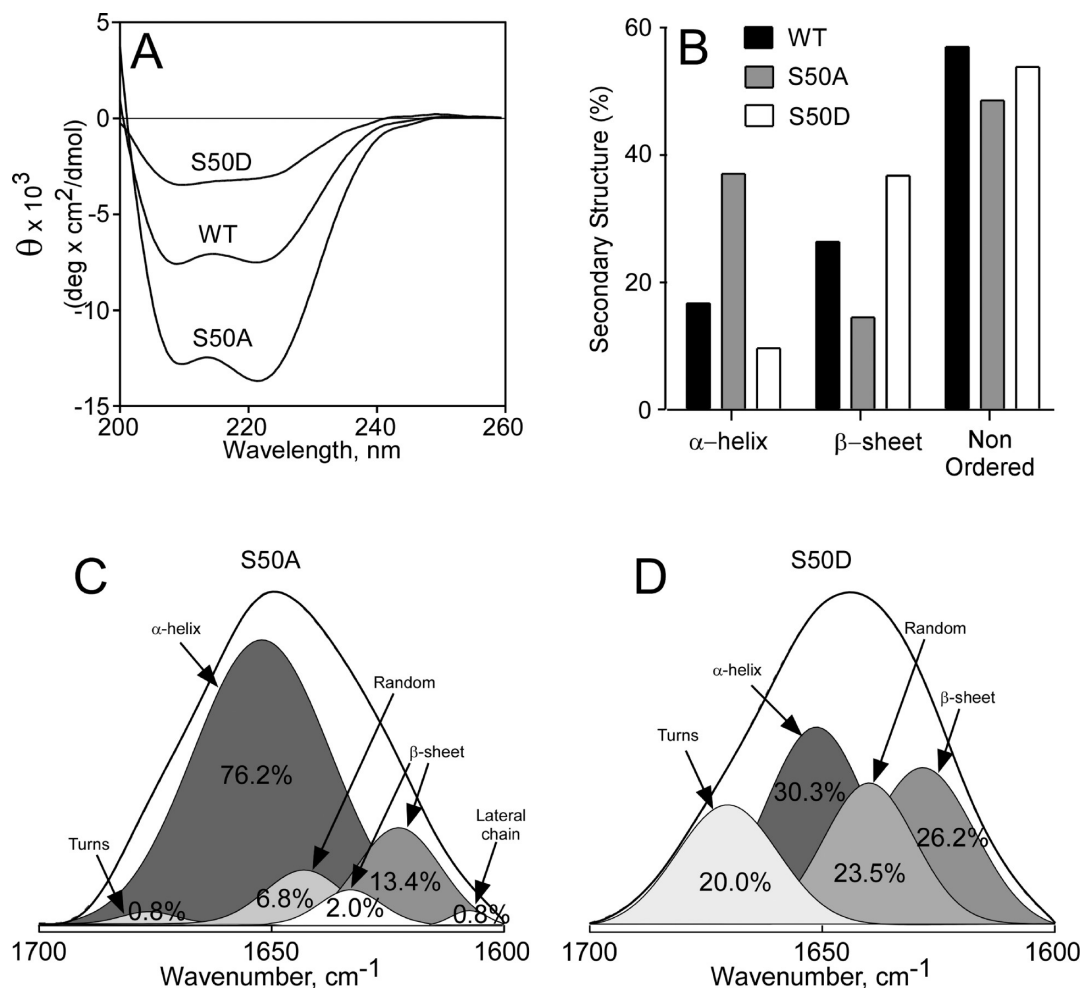
Figure 4. Structural characterization of S50A and S50D mutants. (A) Far-UV CD spectra of the wild type and S50A and S50D mutants in phosphate buffer (pH 7.0). The protein concentration was 15 μM. (B) Percentage of secondary structure elements inferred from the CD spectra determined using the DICHROWEB algorithm. (C and D) FTIR spectra of S50D and S50A mutants in phosphate buffer (pH 7.0). The protein concentration was 1.0 mM. The spectra were deconvoluted in the percentages of secondary structure elements, displayed as individual Gaussian-like graphs.

We evaluated the structure and thermal stability of both mutant proteins by CD and FTIR. As depicted in Figure 4A, the far-UV CD spectra S50A and S50D mutants at 15 μM displayed minima at 208 and 222 nm, and a maximum at 195 nm, akin to those of the wild type. However, the spectrum of the S50A mutant was approximately 2-fold more intense than that of Snapin, while S50D exhibited an intensity that was half of that displayed by the wild type. Indeed, the deconvolution of the far-UV spectra by the DICHROWEB algorithm[44,45] yielded an average α-helix content of 35−40% for S50A and 5−10% for S50D as compared with the value of 15−20% for the wild type (Figure 4B), implying that phosphorylation of S50D notably reduces the level of α-helical secondary structure. These results were corroborated when the secondary structure was studied by FTIR at 1 mM. The infrared spectra displayed a significant shift in the maximum toward the 1650 cm^{-1} region in the S50A mutant, but not for the S50D protein (Figure 4C,D). Self-deconvolution of the spectra indicates a 76% α-helical secondary structure content for the S50A mutant and a 30% content for S50D (Figure 4C,D). Accordingly, incorporation of an Asp into the position of Ser-50 notably reduced the secondary structure content of the protein. In addition, incorporation of a negatively charged residue at Ser-50 appears to affect the formation of higher-order oligomers

(i.e., tetramers), as suggested by the decrease in the ellipticity ratio [$\theta_{222}/\theta_{208}$ values of 0.89 for S50D, 1.01 for the wild type, and 1.12 for S50A (Figure 4A)].[43]

We next studied the thermal stability of these mutants. Thermal melting curves, followed as the change in the ellipticity at 222 nm in the far-UV CD for both S50A and S50D at 15 μM, exhibited sigmoidal behavior with midpoint temperatures (T_m) of 64.2 $\pm$ 0.2 °C for S50A and 59.7 $\pm$ 17.1 °C for S50D (Figure 5A,B), indicating a lower thermal stability of the S50D mutant, which is consistent with its lower α-helical secondary structure content. Note that the T_m of S50D displays a large uncertainty mainly because of the large noise exhibited by the thermal denaturation curve (Figure 5B). Nonetheless, these observations were corroborated by the FTIR-monitored thermal denaturation of the proteins that disclosed a melting temperature for the S50A mutant of 72.8 °C and for the S50D mutant of 56.3 °C (Figure 5C).

Evaluation of the heat-induced unfolding at micromolar concentrations revealed that denaturation of the S50A mutant was highly reversible, losing only 3% of the protein upon being heated to 95 °C (Figure 5D), as compared with the 10% loss of ellipticity at 222 nm by the wild-type protein. The sigmoidal shape of the denaturation curve was not affected, and the T_m of the refolded protein was identical to that of its native
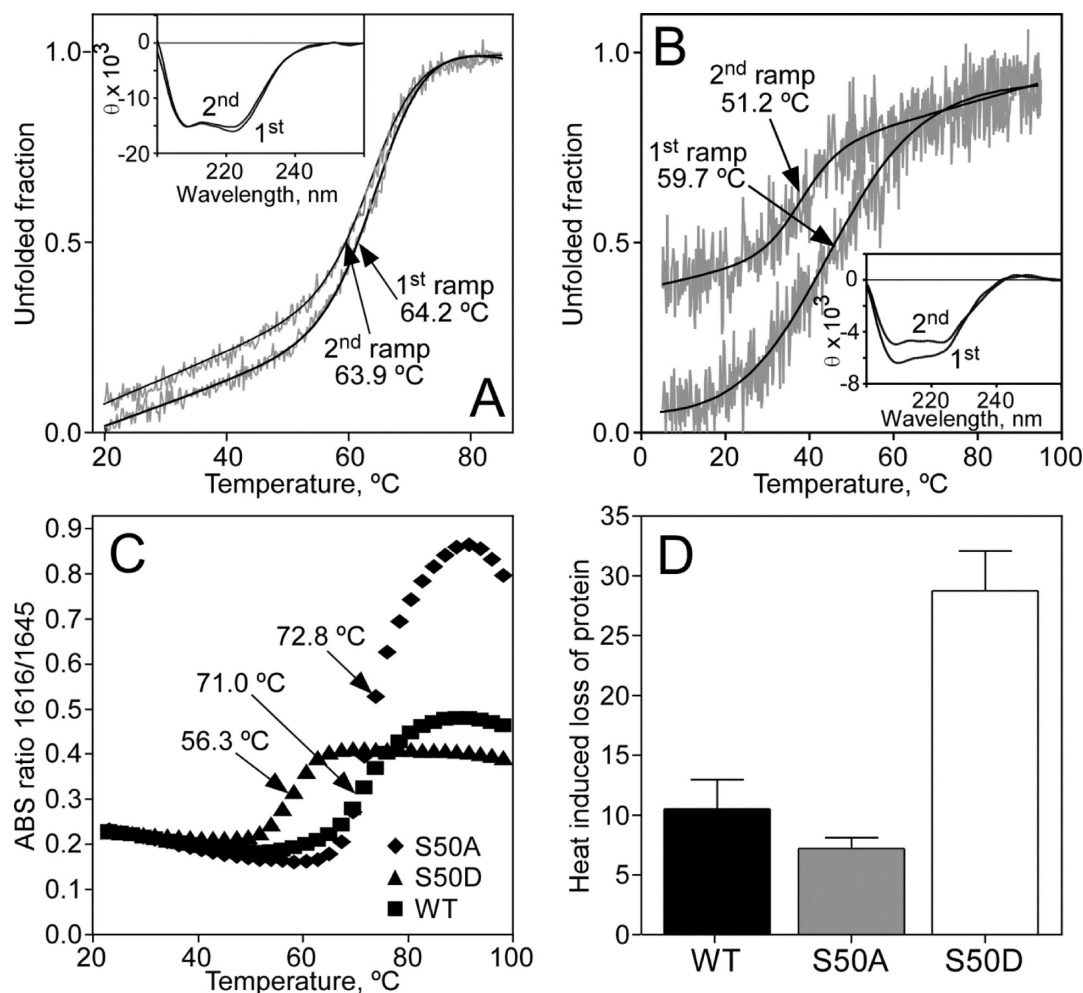
Figure 5. Thermal stability of S50A and S50D mutants. (A and B) Normalized fraction of the unfolded protein as a function of the thermal melting and refolding for S50A and S50D mutants, respectively. The insets shows the thermal denaturation of native (1st) and refolded proteins (2nd), monitored by following the ellipticity at 222 nm of S50A and S50D, respectively. Refolded proteins refer to a protein sample that has been thermally denaturated using a ramp protocol and refolded by incubation at 25 °C. (C) Thermal unfolding measured by FTIR as the change in the ratio of band intensities at 1616 and 1645 cm^{-1} at increasing temperatures. The protein concentration was 1.0 mM. The T_m of each sigmoidal transition was calculated by fitting the curves to a two-state model. (D) Percentage of the loss of secondary structure of the protein upon sample refolding at 25 °C.

counterpart (63.9 °C) (Figure 5A). In contrast, however, the S50D mutant displayed significant thermal lability as evidenced by the loss of ~30% of the molar ellipticity at 222 nm after incubation at 95 °C (Figure 5B,D). The T_m of the refolded protein was lower (51.2 °C) than that of the parental protein (Figure 5B). Taken together, all these findings indicate a lower stability for the S50D mutant and imply that phosphorylation of Ser-50 notably impacts the structure and stability of the protein.

Snapin and Its Mutants Bind with Low Affinity to Recombinant SNAP-25 and the Reconstituted SNARE Complex. Whether Snapin is able to bind to SNAP-25 in vitro is still under debate. The first studies using GST-SNAP-25 pull-down experiments showed the existence of binding with a 1:1 stoichiometry, and saturation reached at 100 nM Snapin.[13,18,23] However, in vitro studies conducted using steady-state far-UV CD and pull-down experiments with recombinant proteins indicated that Snapin was unable to associate with recombinant SNAP-25.[14] Here, we further investigated this question and analyzed the binding of Snapin to SNAP-25. First, we concentrated on the wild-type protein and used the far-UV measurements following the ellipticity of Snapin and SNAP-25

alone, as well as mixed together. As illustrated in Figure 6A, the molar ellipticity of the protein mixture was more intense than that corresponding to the sum of the ellipticities of the individual proteins, implying the presence of a protein complex.[47] Similarly, the infrared spectra obtained in the presence of both proteins display a significant shift of the maximum toward 1650 cm^{-1}, consistent with an increase in the α-helical content of the protein mixture as compared when both proteins are evaluated separately (Figure 6B and Figure S3 of the Supporting Information). Additional support for the formation of the complex arose from thermal denaturation assays of the individual and complexed proteins (Figure 6C). FTIR-monitored thermal denaturation showed that Snapin was denaturated at 71 °C, while SNAP-25 did not show any discernible thermal transition,[47] consistent with its higher content of random secondary structural elements (Figure S3, Supporting Information). In contrast, the melting temperature of the protein mixture (1:1) was 104 °C, which represents a 33 °C stabilization of its thermal stability. This enhanced stability is likely due to the formation of a protein complex. The affinity constant of the complex, inferred from the changes in the intrinsic fluorescence of SNAP-25 upon binding, was
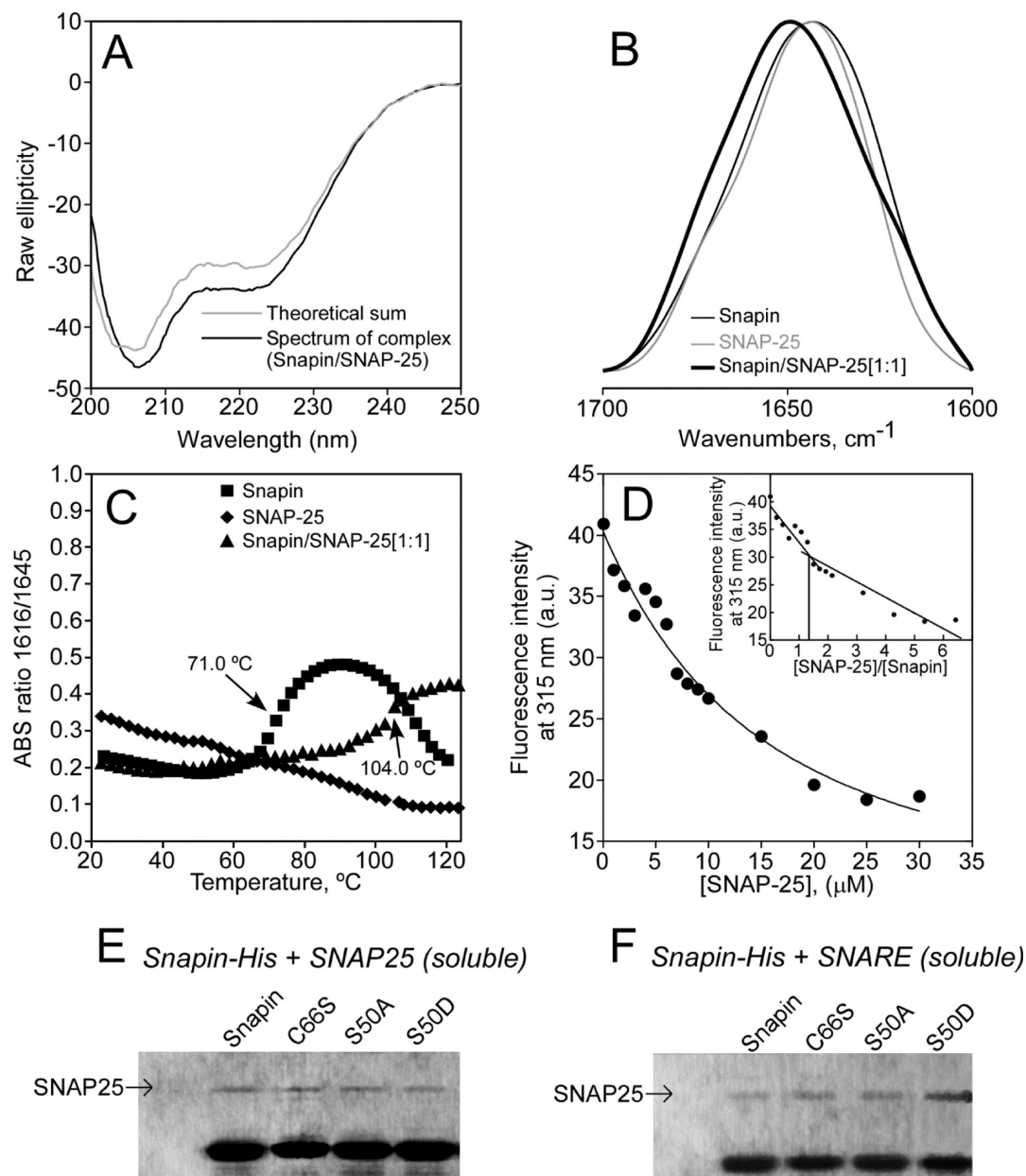
Figure 6. Binding of Snapin to SNAP-25. (A) Far-UV CD spectra of the complex formed by equimolar amounts (2.5 μM) of Snapin and SNAP-25 and the sum spectrum obtained by addition of the spectra of the individual proteins. (B) FTIR spectra of Snapin, SNAP-25, and an equimolar mixture of both proteins. The total protein concentration was 1.0 mM. Spectra were recorded at pH 7.0. (C) Thermal melting of the Snapin−SNAP-25 complex followed by FTIR. Thermal unfolding of isolated Snapin and SNAP-25 was included for comparison. The T_m value of each sigmoidal transition is indicated (the decrease in the magnitude of the signal for Snapin above 100 °C may be due to protein aggregation). (D) Fluorescence titration curves of SNAP-25 with wild-type Snapin followed from the changes in intensity at 315 nm after excitation at 280 nm (similar titration curves were obtained from excitation at 295 nm and collection of data at 330 or 350 nm). The spectroscopic experiments were conducted at 25 °C. (E and F) Pull-down gels of SNAP-25 and the in vitro reconstituted SNARE complex with wild-type and mutant Snapin proteins, respectively.

20 ± 10 μM (Figure 6D), with a stoichiometry of 1:1, estimated from Job's plot[29] (Figure 6D, inset), where the fluorescence intensity as a function of the SNAP-25:Snapin concentration ratio yielded two lines that intersected at an *x* value of 1.2 ± 0.6. Therefore, these findings indicate that Snapin interacts in vitro with recombinant SNAP-25 but that this interaction displays a moderate-to-low association constant.

The formation of the Snapin−SNAP-25 complex was further evaluated biochemically. Immobilized His-Snapin was able to retain SNAP-25, consistent with the formation of a complex (Figure 6E). However, the extent of complex assembly was very modest, amounting to <30% of the input SNAP-25 protein.

A similar modest interaction was obtained (<30% of the input Snapin protein) when the GST-SNAP-25 was immobilized, and its capacity to interact with Snapin was evaluated (data not shown). These results are consistent with the modest-to-low affinity of the interaction that would result in the virtual loss of 80% of the assembled complex after the washing steps, in agreement with observations reported by other groups.[14]

We next investigated biochemically the capacity of the Snapin mutants to interact with recombinant SNAP-25. As seen in Figure 6E, the three mutants C66S, S50A, and S50D were able to associate with SNAP-25, although like that of the wild-type protein, the extent of the interaction was modest (<30% of

the input SNAP-25 protein bound to the immobilized proteins), in agreement with a low affinity of the proteins. Quantification of the protein bands and normalization with respect to the His-Snapin input protein show that none of the mutations significantly augmented or diminished the amount of SNAP-25 bound (Table 1).

Table 1. Densitometric Analysis of SNAP-25 and SNARE Complex Pull-Down Experiments with Snapin Species

	SNAP-25[a]	SNARE[b]
Snapin	0.28 ± 0.07	0.31 ± 0.08
C66S	0.35 ± 0.08	0.42 ± 0.10
S50A	0.32 ± 0.09	0.39 ± 0.11
S50D	0.24 ± 0.11	0.65 ± 0.18^{c}

[a]Quantification of the SNAP-25 band of a pull-down gel of free SNAP-25 with immobilized His-Snapin (Figure 6E). [b]Quantification of the SNAP-25 band of a pull-down gel of the SNARE complex with immobilized His-Snapin (Figure 6F). Data are represented as the ratio of SNAP-25 to His-Snapin displayed in the gel. His-Snapin was used as a loading control. Data are given as means $\pm$ standard deviation from three independent experiments. $^{c}p < 0.05$ using a Student's t test.

Because Snapin in cells binds to the SNARE complex, rather than SNAP-25, we questioned whether the interaction of the protein with the in vitro reconstituted SNARE complex was affected by mutation at Cys-66 or Ser-50. For this experiment, His-Snapin species were immobilized in NTA-agarose, and the ability to retain the reconstituted SNARE complex was assessed. Figure 6F shows that all Snapin species interacted with the SNARE complex. The level of SNARE binding to wild-type Snapin protein was modest, ~0.30 (Table 1). A similar result was obtained for the C66S and S50A mutants. In contrast, we observed that mutant S50D displayed a ratio of 0.65, which represents a 2-fold increase compared with that of the wild type, implying a stronger interaction of this mutant with the reconstituted SNARE complex, in accordance with results obtained with phosphorylated Snapin.[16] Nonetheless, note that the level of complex formation is low (<40% of the input SNARE complex for the S50D mutant), suggesting that in vitro these recombinant proteins associate with low affinity.

■ DISCUSSION

The main aim of this study was to gain structural insights into Snapin, a protein that has been described as an interacting partner of the SNARE fusion complex that is involved in modulating regulated exocytosis,[13] as well as the function of other proteins such as TRP channels.[20,21] Snapin is a predicted membrane protein of 15 kDa that exhibits a short hydrophobic domain at the N-terminus, presumably responsible for its attachment to the vesicular membrane, and a cytosolic C-terminus predicted to form coiled coils. In addition, Snapin contains two residues that have been signaled as being critical for its biological function, namely, the Cys-66 residue involved in protein dimerization[18] and the Ser-50 residue that is phosphorylated by PKA modulating protein function.[16,17] Thus, we investigated the structural features and stability of Snapin and mutants C66S, S50A, and S50D, along with their interaction in vitro with SNAP-25 and the reconstituted SNARE complex. Mutations S50A and S50D have been show to mimic the function of the nonphosphorylated and phosphorylated forms of Snapin.[16,17]

A salient contribution of this study is the finding that recombinant Snapin is an oligomeric protein that is present in solution mainly as dimers in equilibrium with tetramers. This finding contrasts with previous reports indicating that Snapin is a dimer with no evidence of higher-order oligomers, as concluded from size-exclusion chromatography.[14] This discrepancy in the oligomeric state of the protein is intriguing, because our size-exclusion profile is consistent with the presence of higher-order oligomeric species in purified recombinant Snapin solutions. A plausible explanation may be the different chromatographic column used in these studies, namely, a Superdex 200 column in ref 14 and a Superdex 75 column in our study. In support of this notion, the chromatogram obtained with the Superdex 200 column displays a very broad peak, as compared with the narrow peaks we obtained (Figure 1A). Furthermore, we cannot rule out the possibility that our experimental conditions, i.e., a low salt concentration, also contributed to the formation of the higher-order Snapin oligomers. Note that the presence of higher-order oligomers was also supported by AU that revealed the presence of dimers in equilibrium with tetramers. Noteworthy is the fact that abrogation of disulfide-mediated protein dimerization did not abolish the formation of tetramers as revealed also by size-exclusion chromatography and AU. Taken together, we conclude that recombinantly produced Snapin is a dimeric protein with a tendency to assemble into tetramers probably mediated by the formation of a coiled-coil bundle. We cannot rule out at present the possibility that the transmembrane domain of Snapin could contribute to the higher-order oligomers, although it seems unlikely to us that a highly specific oligomerization state (tetramer) could be solely due to the presence of a hydrophobic chain.

Unexpectedly, structural analysis of the wild-type protein by CD revealed a notable low level of secondary structure, consistent with the tenet that Snapin may be a naturally unfolded protein in solution. This lack of protein secondary structure was more evident at low concentrations like those used in CD experiments. An increase in the protein concentration gave rise to a 2-fold increase in protein secondary structure content, that is, mainly its α-helical content, as shown by FTIR analysis. Because an increase in the protein concentration would favor the assembly of high-order oligomers (Le Chatelier's principle), this result suggests that the tetrameric form of the protein has a larger amount of secondary structure. In support of this notion, the C66S mutant displays 2-fold more α-helical content than the wild-type protein, in agreement with its stronger propensity to assemble as tetramers. In marked contrast, Vites et al.[14] found that wild-type Snapin displays a very high α-helical content in solution (64%) when determined at low protein concentrations. We do not have an explanation for this discrepancy, because in our hands, Snapin helical content, determined by two complementary techniques (CD and FTIR), did not surpass 37% at high concentrations. Intriguingly, however, the thermal stabilities of our protein and that of Vites et al.[14] were similar, as both displayed an unfolding transition temperature of 58 °C at micromolar concentrations and the heat-induced unfolding process is largely reversible. Moreover, we observe a significant 13 °C increase in the melting temperature of the protein when its concentration is increased at 1 mM, concomitant to the increment in helical content. A similar result is observed with the C66S mutant, which, in addition, exhibits unfolding transition temperatures higher than that of wild-type Snapin.

Taken together, these findings imply that the structure detected in recombinant, purified Snapin may probably arise from the population of tetrameric assemblies and that dimeric and/or monomeric species are rather unordered or exhibit an unstable structure that could be stabilized either by dimer–dimer association or by the interaction with other proteins. This structural flexibility may underlie the interaction of the protein with multiple and diverse partners.[48,49]

The cellular activity of Snapin is modulated by PKA that phosphorylates Ser-50,[16,17] promoting the interaction of the protein with the SNARE complex.[16] Hence, the question of what structural consequences, if any, cause the improvement in the function of the phosphorylated protein arises. We addressed this issue by characterizing the structural and thermal stabilities of two mutants, S50A and S50D, that emulate the unphosphorylated and phosphorylated species.[16,17] As expected, our results show that S50A is quite similar to the wild-type protein, although it displays significantly higher α-helical content and thermal stability, suggesting that incorporation of an alanine residue at this position augments the formation of well-ordered tetramers in solution. This increase in helical structure content promoted by alanine is consistent with the stronger helical propensity exhibited by this residue as compared with serine.[50] In marked contrast, the S50D mutant exhibited a significantly lower secondary structure content that it is accompanied by a lower thermal stability. In addition, and more remarkably, this mutant exhibited a rather irreversible thermal denaturation, as evidenced by the notable loss of secondary structure of the protein upon heat-induced unfolding. These properties may be explained if incorporation of a negative charge in this position destabilizes the formation of protein tetramers, thus favoring the presence of the unordered species. Accordingly, the higher activity of phosphorylated Snapin could arise at least in part from a destabilization of the formation of stable tetrameric assemblies, consistent with the notion that the active form of the protein is the dimer.[18]

Snapin was identified as an interacting partner of SNAP-25 and the SNARE complex. This interaction appears to be critical for the function of the protein.[13,18] However, some controversy about whether the interaction occurs or is just an unspecific, electrostatically mediated association exists.[14] We addressed this question and evaluated the formation of protein complexes between SNAP-25 and Snapin species. Our findings indicate that the wild-type protein bound to the SNARE protein, in agreement with previous reports.[13,18] This assertion was derived from (i) the higher α-helical content and (ii) the higher thermal stability of a mixture containing both proteins as compared with those of samples of individual proteins. The interaction, however, was weak, with an apparent affinity in the micromolar range and a 1:1 stoichiometry for the protein complex, although the existence of larger assemblies cannot be completely ruled out. This is also in agreement with the weak capacity of immobilized Snapin to pull down SNAP-25 and the reconstituted SNARE complex. Noteworthy, however, was our observation that the S50D mutant displayed an appreciably stronger interaction with the SNARE complex, as evidenced by the larger SNARE complex pull down. The other mutant proteins, S50A and C66S, interacted with the SNARE proteins to a level similar to that of the wild-type protein. Accordingly, our results suggest that in vitro purified Snapin loosely interacts with SNARE proteins and that this interaction is marginal but became significantly stronger via incorporation of a negatively charged residue at Ser-50, in agreement with the stronger

interaction with SNARE proteins observed for the PKA-phosphorylated and S50D proteins.[16] It should be mentioned that protein species that tend to increase the helical content and thermal stability of the protein (C66A and S50A) exhibit impaired function,[17,18] while those that decrease the secondary structure content and thermal stability (S50D) display enhanced functionality.[16] Thus, the higher cellular activity of the phosphorylated and S50D species might arise at least in part from the destabilizing effect that the covalent modification (i.e., phosphorylation) has on the tendency of Snapin to form tetrameric assemblies.

In conclusion, we have provided evidence that Snapin is oligomeric in solution and that these multimers are rather ordered and stable proteins, capable of binding to SNAP-25 with low affinity as well as to the SNARE complex. Abrogation of disulfide-linked dimers produces mainly tetrameric oligomers in solution, with a higher content of secondary structure and higher thermal stability. In contrast, mutation of Ser-50 to Asp appears to destabilize the protein structure, possibly by favoring the presence of protein dimers that may be characterized by a relatively unordered structure and low thermal stability. These characteristics, however, might be pivotal in defining its stronger binding to the SNARE complex and, therefore, the higher activity of phosphorylated species. Nonetheless, it should be noted that high-order oligomers have been observed using purified Snapin in solution, which contrasts with the membrane-attached form present in cells. In this regard, it remains to be explored whether membrane-tethered Snapin dimers retain the propensity to oligomerize through the formation of a coiled-coil bundle.

■ ASSOCIATED CONTENT

Ⓢ Supporting Information
One figure depicting the amide II region of the C66S mutant, a second figure displaying the thermal denaturation of Snapin and the C66S mutant followed by FTIR, and a third figure displaying the FTIR analysis of Snapin and SNAP-25 proteins. This material is available free of charge via the Internet at http://pubs.acs.org.

■ AUTHOR INFORMATION

Corresponding Author
*Instituto de Biología Molecular y Celular, Universidad Miguel Hernández, 03202 Elche (Alicante), Spain. Telephone: (+34) 966658727. Fax: (+34) 966658758. E-mail: aferrer@umh.es.

Notes
The authors declare no competing financial interest.

■ ABBREVIATIONS
PKA, protein kinase A; SNAP-25, synaptosome-associated protein of 25 kDa; Syt-I, synaptotagmin-I; TRP, transient

receptor potential; CD, circular dichroism; FTIR, Fourier transform infrared spectroscopy; DTT, dithiothreitol; AU, analytical ultracentrifugation; β-MSH, β-mercaptoethanol.

■ REFERENCES

(1) Sudhof, T. C. (2004) The synaptic vesicle cycle. *Annu. Rev. Neurosci. 27*, 509−547.

(2) Sudhof, T. C., and Rothman, J. E. (2009) Membrane fusion: Grappling with SNARE and SM proteins. *Science 323*, 474−477.

(3) Wojcik, S. M., and Brose, N. (2007) Regulation of membrane fusion in synaptic excitation-secretion coupling: Speed and accuracy matter. *Neuron 55*, 11−24.

(4) Chen, Y. A., and Scheller, R. H. (2001) SNARE-mediated membrane fusion. *Nat. Rev. Mol. Cell Biol. 2*, 98−106.

(5) Calakos, N., Bennett, M. K., Peterson, K. E., and Scheller, R. H. (1994) Protein-protein interactions contributing to the specificity of intracellular vesicular trafficking. *Science 263*, 1146−1149.

(6) Huntwork, S., and Littleton, J. T. (2007) A complexin fusion clamp regulates spontaneous neurotransmitter release and synaptic growth. *Nat. Neurosci. 10*, 1235−1237.

(7) Schoch, S., Castillo, P. E., Jo, T., Mukherjee, K., Geppert, M., Wang, Y., Schmitz, F., Malenka, R. C., and Sudhof, T. C. (2002) RIM1α forms a protein scaffold for regulating neurotransmitter release at the active zone. *Nature 415*, 321−326.

(8) Xue, M., Ma, C., Craig, T. K., Rosenmund, C., and Rizo, J. (2008) The Janus-faced nature of the C(2)B domain is fundamental for synaptotagmin-1 function. *Nat. Struct. Mol. Biol. 15*, 1160−1168.

(9) Shin, O. H., Xu, J., Rizo, J., and Sudhof, T. C. (2009) Differential but convergent functions of Ca^{2+} binding to synaptotagmin-1 C2 domains mediate neurotransmitter release. *Proc. Natl. Acad. Sci. U.S.A. 106*, 16469−16474.

(10) Chapman, E. R. (2008) How does synaptotagmin trigger neurotransmitter release? *Annu. Rev. Biochem. 77*, 615−641.

(11) Tucker, W. C., Edwardson, J. M., Bai, J., Kim, H. J., Martin, T. F., and Chapman, E. R. (2003) Identification of synaptotagmin effectors via acute inhibition of secretion from cracked PC12 cells. *J. Cell Biol. 162*, 199−209.

(12) Bai, J., Wang, C. T., Richards, D. A., Jackson, M. B., and Chapman, E. R. (2004) Fusion pore dynamics are regulated by synaptotagmin*t-SNARE interactions. *Neuron 41*, 929−942.

(13) Ilardi, J. M., Mochida, S., and Sheng, Z. H. (1999) Snapin: A SNARE-associated protein implicated in synaptic transmission. *Nat. Neurosci. 2*, 119−124.

(14) Vites, O., Rhee, J. S., Schwarz, M., Rosenmund, C., and Jahn, R. (2004) Reinvestigation of the role of snapin in neurotransmitter release. *J. Biol. Chem. 279*, 26251−26256.

(15) Ruder, C., Reimer, T., Delgado-Martinez, I., Hermosilla, R., Engelsberg, A., Nehring, R., Dorken, B., and Rehm, A. (2005) EBAG9 adds a new layer of control on large dense-core vesicle exocytosis via interaction with Snapin. *Mol. Biol. Cell 16*, 1245−1257.

(16) Chheda, M. G., Ashery, U., Thakur, P., Rettig, J., and Sheng, Z. H. (2001) Phosphorylation of Snapin by PKA modulates its interaction with the SNARE complex. *Nat. Cell Biol. 3*, 331−338.

(17) Thakur, P., Stevens, D. R., Sheng, Z. H., and Rettig, J. (2004) Effects of PKA-mediated phosphorylation of Snapin on synaptic transmission in cultured hippocampal neurons. *J. Neurosci. 24*, 6476−6481.

(18) Pan, P. Y., Tian, J. H., and Sheng, Z. H. (2009) Snapin facilitates the synchronization of synaptic vesicle fusion. *Neuron 61*, 412−424.

(19) Starcevic, M., and Dell'Angelica, E. C. (2004) Identification of snapin and three novel proteins (BLOS1, BLOS2, and BLOS3/ reduced pigmentation) as subunits of biogenesis of lysosome-related organelles complex-1 (BLOC-1). *J. Biol. Chem. 279*, 28393−28401.

(20) Morenilla-Palao, C., Planells-Cases, R., Garcia-Sanz, N., and Ferrer-Montiel, A. (2004) Regulated exocytosis contributes to protein kinase C potentiation of vanilloid receptor activity. *J. Biol. Chem. 279*, 25665−25672.

(21) Krapivinsky, G., Mochida, S., Krapivinsky, L., Cibulsky, S. M., and Clapham, D. E. (2006) The TRPM7 ion channel functions in cholinergic synaptic vesicles and affects transmitter release. *Neuron 52*, 485−496.

(22) Buxton, P., Zhang, X. M., Walsh, B., Sriratana, A., Schenberg, I., Manickam, E., and Rowe, T. (2003) Identification and characterization of Snapin as a ubiquitously expressed SNARE-binding protein that interacts with SNAP23 in non-neuronal cells. *Biochem. J. 375*, 433−440.

(23) Tian, J. H., Wu, Z. X., Unzicker, M., Lu, L., Cai, Q., Li, C., Schirra, C., Matti, U., Stevens, D., Deng, C., Rettig, J., and Sheng, Z. H. (2005) The role of Snapin in neurosecretion: Snapin knock-out mice exhibit impaired calcium-dependent exocytosis of large dense-core vesicles in chromaffin cells. *J. Neurosci. 25*, 10546−10555.

(24) Valente, P., García-Sanz, N., Gomis, A., Fernández-Carvajal, A., Fernández-Ballester, G., Viana, F., Belmonte, C., and Ferrer-Montiel, A. (2008) Identification of molecular determinants of channel gating in the transient receptor potential box of vanilloid receptor I. *FASEB J. 222*, 3298−3309.

(25) Miroux, B., and Walker, J. E. (1996) Over-production of proteins in *Escherichia coli*: Mutant hosts that allow synthesis of some membrane proteins and globular proteins at high levels. *J. Mol. Biol. 260*, 289−298.

(26) Gill, S. C., and von Hippel, P. H. (1989) Calculation of protein extinction coefficients from amino acid sequence data. *Anal. Biochem. 182*, 319−326.

(27) Alcaraz, L. A., del Álamo, M., Barrera, F. N., Mateu, M. G., and Neira, J. L. (2007) Flexibility in HIV-1 assembly subunits: Solution structure of the monomeric C-terminal domain of the capsid protein. *Biophys. J. 93*, 1264−1276.

(28) Blanes-Mira, C., Merino, J. M., Valera, E., Fernandez-Ballester, G., Gutierrez, L. M., Viniegra, S., Perez-Paya, E., and Ferrer-Montiel, A. (2004) Small peptides patterned after the N-terminus domain of SNAP25 inhibit SNARE complex assembly and regulated exocytosis. *J. Neurochem. 88*, 124−135.

(29) Facchiano, A., and Ragone, R. (2003) Modification of Job's method for determining the stoichiometry of protein-protein complexes. *Anal. Biochem. 313*, 170−172.

(30) Muro-Pastor, M. I., Barrera, F. N., Reyes, J. C., Florencio, F. J., and Neira, J. L. (2003) The inactivating factor of glutamine synthetase, IF7, is a "natively unfolded" protein. *Protein Sci. 12*, 1443−1454.

(31) Woody, R. W. (1995) Circular dichroism. *Methods Enzymol. 246*, 34−71.

(32) Encinar, J. A., Mallo, G. V., Mizyrycki, C., Giono, L., Gonzalez-Ros, J. M., Rico, M., Canepa, E., Moreno, S., Neira, J. L., and Iovanna, J. L. (2001) Human p8 is a HMG-I/Y-like protein with DNA binding activity enhanced by phosphorylation. *J. Biol. Chem. 276*, 2742−2751.

(33) Echabe, I., Encinar, J. A., and Arrondo, J. L. R. (1997) Removal of spectral noise in the quantitation of protein structure through infrared band decomposition. *Biospectroscopy 3*, 469−475.

(34) Piotto, M., Saudek, V., and Sklenar, V. (1992) Gradient-tailored excitation for single-quantum NMR spectroscopy of aqueous solutions. *J. Biomol. NMR 2*, 661−665.

(35) Czypionka, A., de los Panos, O. R., Mateu, M. G., Barrera, F. N., Hurtado-Gomez, E., Gomez, J., Vidal, M., and Neira, J. L. (2007) The isolated C-terminal domain of Ring1B is a dimer made of stable, well-structured monomers. *Biochemistry 46*, 12764−12776.

(36) Wilkins, D. K., Grimshaw, S. B., Receveur, V., Dobson, C. M., Jones, J. A., and Smith, L. J. (1999) Hydrodynamic radii of native and denatured proteins measured by pulse field gradient NMR techniques. *Biochemistry 38*, 16424−16431.

(37) Schuck, P. (2000) Size-distribution analysis of macromolecules by sedimentation velocity ultracentrifugation and Lamm equation modeling. *Biophys. J. 78*, 1606−1619.

(38) Laue, T. M. S., Ridgeway, T. M., and Pelletier, S. L. (1992) Computer-aided Interpretation of Analytical Sedimentation Data For Proteins. In *Analytical Ultracentrifugation in Biochemistry and Polymer Science* (Harding, S. E., Rowe, A. J., and Horton, J. C., Eds.) pp 90−125, The Royal Society of Chemistry, Cambridge, U.K.

(39) Minton, A. P. (1994) Conservation of signal: A new algorithm for the elimination of the reference concentration as an independently variable parameter in the analysis of sedimentation equilibrium. In *Modern analytical ultracentrifugation* (Schuster, T. H., and Lave, T. H., Eds.) pp 81−92, Birkhaüser, Boston.

(40) Kelly, S. M., and Price, N. C. (2000) The use of circular dichroism in the investigation of protein structure and function. *Curr. Protein Pept. Sci. 1*, 349−384.

(41) Casares, S., Sadqi, M., Lopez-Mayorga, O., Conejero-Lara, F., and van Nuland, N. A. (2004) Detection and characterization of partially unfolded oligomers of the SH3 domain of α-spectrin. *Biophys. J. 86*, 2403−2413.

(42) Atkins, P. W., and De Paula, J. (2006) *Physical Chemistry*, Oxford University Press, Oxford, U.K.

(43) Cooper, T. M., and Woody, R. W. (1990) The effect of conformation on the CD of interacting helices: A theoretical study of tropomyosin. *Biopolymers 30*, 657−676.

(44) Whitmore, L., and Wallace, B. A. (2004) DICHROWEB, an online server for protein secondary structure analyses from circular dichroism spectroscopic data. *Nucleic Acids Res. 32*, W668−W673.

(45) Whitmore, L., and Wallace, B. A. (2008) Protein secondary structure analyses from circular dichroism spectroscopy: Methods and reference databases. *Biopolymers 89*, 392−400.

(46) Wüthrich, K. (1986) *NMR of proteins and nucleic acids*, John Wiley & Sons, Inc., New York.

(47) Fasshauer, D., Antonin, W., Margittai, M., Pabst, S., and Jahn, R. (1999) Mixed and non-cognate SNARE complexes. Characterization of assembly and biophysical properties. *J. Biol. Chem. 274*, 15440−15446.

(48) Tompa, P. (2002) Intrinsically unstructured proteins. *Trends Biochem. Sci. 27*, 527−533.

(49) Dyson, H. J., and Wright, P. E. (2005) Intrinsically unstructured proteins and their functions. *Nat. Rev. Mol. Cell Biol. 6*, 197−208.

(50) Pace, C. N., and Scholtz, J. M. (1998) A helix propensity scale based on experimental studies of peptides and proteins. *Biophys. J. 75*, 422−427.